Theoretical study of a cold atom beam splitter

Naceur Gaaloul, Annick Suzor-Weiner, Laurence Pruvost, Mourad Telmini, Eric Charron

Theoretical study of a cold atom beam splitter

Naceur Gaaloul[1,3], Annick Suzor-Weiner[1], Laurence Pruvost[2], Mourad Telmini[3] and Eric Charron[1]
[1] *Laboratoire de Photophysique Moléculaire, CNRS, Bâtiment 210, Université Paris Sud, 91405 Orsay cedex, France.*
[2] *Laboratoire Aimé Cotton, CNRS, Bâtiment 505, Université Paris Sud, 91405 Orsay cedex, France.*
[3] *Laboratoire de Spectroscopie Atomique, Moléculaire et Applications, Department of Physics, Faculty of Sciences of Tunis, University Tunis El Manar, 2092 Tunis, Tunisia.*
(Dated: January 20, 2006)

A theoretical model is presented for the study of the dynamics of a cold atomic cloud falling in the gravity field in the presence of two crossing dipole guides. The cloud is splitted between the two branches of the guide, and we compare experimental measurements of the splitting efficiency with semi-classical simulations. We then explore the possibilities of optimization of this beam splitter. Our numerical study also gives access to detailed informations, such as the atom temperature after the splitting. It finally sets the foundation for a study of the coherence properties of the guided atoms.

I. INTRODUCTION

The manipulation of cold atoms with optical fields is a very promising technique which is rapidly developping in the context of atom optics [1]. Its applications range from laser cooling and trapping [2, 3, 4, 5] to coherent atom transportation [6, 7, 8, 9, 10] and matter wave interferometry [11, 12]. Optical fields have also been proposed as an interesting tool to control the dynamics of internal and motional states of cold atoms for quantum information processing [13, 14, 15, 16, 17], and recent experimental studies have demonstrated a very promising beginning of implementation with optical lattices [18, 19].

For these applications, an effective way of guiding or transporting the atoms while keeping their coherence is required. For atom interferometry it is also necessary to separate the atomic wavefunction between the arms of an interferometer. Several experimental configurations have thus been explored for the implementation of an atom beam splitter with optical potentials [6, 9, 20] as well as with magnetic field potentials [21, 22, 23, 24].

A few theoretical studies of cold atom beam splitters have been published recently in various trapping situations [25, 26, 27]. In these approaches it was assumed that the atomic wave packet was tightly confined in the z-dimension, and the effect of gravity was neglected. In the present article we study the cold atom beam splitter implemented experimentally as in reference [6] by solving numerically the time dependent Schrödinger equation describing the atomic motion in the presence of the gravity field with realistic trapping potentials. Our aim is to propose a theoretical model which can reproduce the main features of this experiment, and to test its pertinence in order to apply it in further more elaborated situations.

A large ensemble of ^{87}Rb atoms is initially trapped and cooled down to a temperature T_0 in a magneto-optical trap (MOT) localized at the altitude $z = 0$ (see Figure 1 for a schematic view). At time $t = 0$, the trapping potential is switched off, while a vertical far off-resonant laser beam crossing the cloud close to its center is switched on. The dipole interaction creates a potential well of depth U_0 which traps a significant portion of the atoms in the transverse directions x and y.

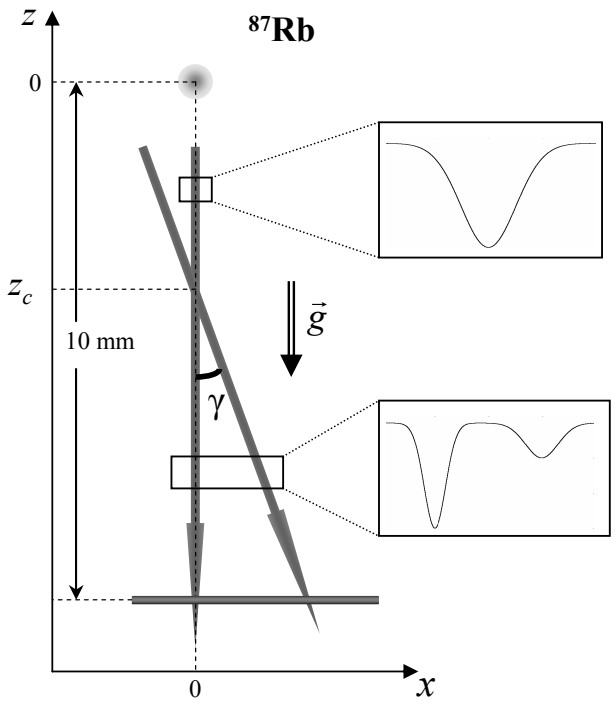

FIG. 1: Schematic view of the guiding setup. The initial ^{87}Rb cloud is shown at the altitude $z = 0$. When the magneto-optic trap is switched off, a vertical laser beam is switched on and the cloud, partially trapped by the associated dipole force, falls in the gravity field. At time t_0 a second oblique guide is switched on. The two guides cross at the altitude z_c and form an angle γ. The trapping potential seen by the atoms at two different altitudes is shown in the insets. Finally, the atoms are probed 1 cm below the initial position.

The guided atoms then fall due to gravity, with a con-

fined dynamics in the x and y directions. At time t_0 a second oblique guide is suddenly switched on. The two guides cross at the altitude z_c and form an angle γ. A potential well, of depth U_1, is induced by the optical dipole interaction with the oblique guide. This creates an additional path for the motion of the atoms. Depending on the various parameters (light intensity, angle γ, temperature T_0, ...) a splitting of the cloud can be observed [6] between the vertical and oblique branches.

II. THEORETICAL MODEL

In order to simplify the numerical treatment of this phenomenon, we restrict the dimensions of this study to the plane defined by the two guiding beams, and therefore to the x and z dimensions only. In addition, we adopt a semi-classical approach, where the effect of the gravity is treated classically. This approximation is justified by the value of the de Broglie wavelength associated with the speed of the particules in the z direction, $\lambda_{\rm db} \sim 1$ Å.

A. Classical approach

A two-dimensional classical trajectory $\{x(t), z(t)\}$ is first evaluated by solving Newton's equations of motion for an atom initially at the position $\{x_0, z_0\}$ with the momentum $\{\dot{x}_0, \dot{z}_0\}$. An efficient variable time-step Runge-Kutta integrator [28] is used to solve these equations in the total potential $V_t(x,z,t) = V_g(x,z,t) + mgz$, where m denotes the atomic mass and g the gravitational constant. The guiding potential $V_g(x,z,t)$ is given by the following sum

$$V_g(x,z,t) = V_0(x) + V_1(x,z,t)\,, \qquad (1)$$

with

$$\left\{ \begin{array}{rcl} V_0(x) & = & -U_0\ \mathrm{e}^{-2\,x^2/w_0^2} \\ V_1(x,z,t) & = & -U_1\ u(t-t_0)\ \mathrm{e}^{-2\,x'^2/w_1^2} \end{array} \right. . \qquad (2)$$

In the previous expressions w_0 and w_1 denote the waists of the vertical and oblique laser beams respectively, and $u(t-t_0)$ stands for the Heaviside step function. The following rotated coordinates

$$\left\{ \begin{array}{rcrcrcl} x' & = & x & \cos\gamma & + & (z-z_c) & \sin\gamma \\ z' & = & (z-z_c) & \cos\gamma & - & x & \sin\gamma \end{array} \right. \qquad (3)$$

have also been introduced (see Figure 2a). The gaussian form of this potential arises from the gaussian intensity profile of the laser beam [6].

Figure 2a shows three typical trajectories with potential parameters close to the one chosen in the experiment performed in Orsay [6]. From this graph it is already clear that, classically, only very specific initial conditions (such as $x_0 = -0.2\,$mm and $z_0 = \dot{x}_0 = \dot{z}_0 = 0$) drive the atom in the oblique branch. Comparing the kinetic energy of

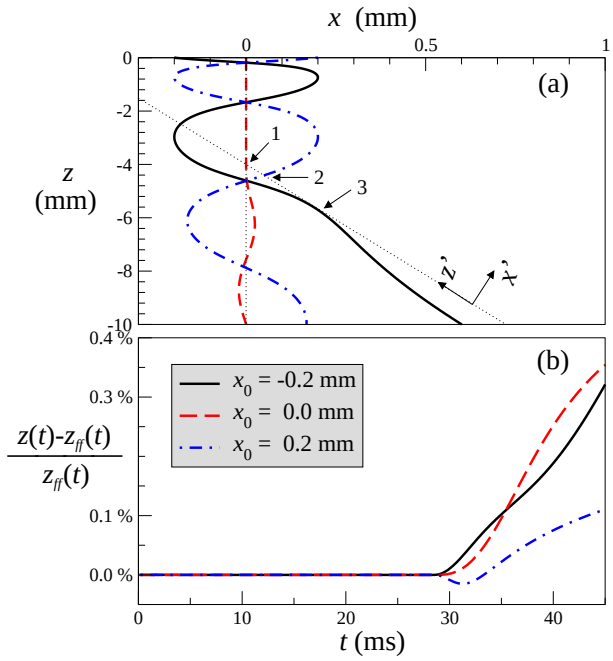

FIG. 2: (Color online) (a) Classical trajectories of a cold atom falling in the gravity field in the presence of the two trapping potentials with $U_0 = 30\,\mu$K, $U_1 = 10\,\mu$K, $w_0 = 0.2\,$mm and $w_1 = 0.3\,$mm. The three trajectories correspond to an initial altitude $z_0 = 0$ and initials positions $x_0 = -0.2\,$mm (black solid line), $x_0 = 0$ (red dashed line) and $x_0 = +0.2\,$mm (blue dash-dotted line) with zero initial momentum ($\dot{z}_0 = 0$ and $\dot{x}_0 = 0$). The two guides cross at the altitude $z_c = -4\,$mm with an angle $\gamma = 0.12\,$rad, and the oblique guide is switched on at $t_0 = 28.6\,$ms. At this date, a free fall dynamics would give the altitude $z_{ff}(t_0) = z_0 - \dot{z}_0 t - \frac{1}{2} g t_0^2 = -4\,$mm corresponding exactly to z_c. Unless specified, these laser parameters remain fixed throughout the paper. The thin vertical and oblique dotted lines reveal the geometry of the laser beams. (b) Deviation of the trajectories from a free fall dynamics in the z-direction for the same initial conditions as in (a).

the atom in the x' direction at time $t = t_0$, $E_{x'}$, with the binding energy of the oblique guide gives the actual criterium which decides in favor or against the deviation of the atom from its natural vertical fall. This can be inferred from Figure 2a : the trajectory induced by the initial condition $x_0 = +0.2\,$mm crosses the oblique guide almost perpendicularly at the point labelled 2 on the graph, with a maximum kinetic energy $E_{x'}$. This trajectory therefore remains almost unaffected by the presence of the oblique laser beam. On the contrary, the trajectory associated with the initial condition $x_0 = -0.2\,$mm meets the oblique guide almost tangentially at the point labelled 3, and the atom is deflected from its initial vertical motion. The intermediate case $x_0 = 0$ follows a dynamics similar to the initial condition $x_0 = +0.2\,$mm with a very slight deviation from the initial vertical motion. It will be shown in section III that this simple interpretation, in terms of individual trajectories, is not valid anymore when the atomic dynamics is treated at

the quantum level.

Finally, Figure 2b shows the deviations of these trajectories from a simple free fall dynamics in the z-direction defined by the classical expression $z_{ff}(t) = z_0 - \dot{z}_0 t - \frac{1}{2} g t^2$. On the time interval $0 \leqslant t \leqslant 45\,\mathrm{ms}$, required to reach the detection probe located at the altitude $z_p = -10\,\mathrm{mm}$, this deviation remains smaller than half a percent, and this justifies the approach adopted in the following, where the dynamics along the z-dimension is simply treated as a classical free fall. We now turn to the description of this semi-classical approach.

B. Semi-classical treatment

In the limit of dilute gases, the dynamics of the cloud can be simulated by solving the time-dependent Schrödinger equation along the x and z dimensions for the wavepacket $\Psi(x,z,t)$ describing the external dynamics of a trapped atom

$$i\hbar \frac{\partial}{\partial t} \Psi(x,z,t) = \hat{\mathcal{H}}_{2\mathrm{D}}(x,z,t)\ \Psi(x,z,t)\,. \tag{4}$$

Since the initial state of the atomic wave packet can be described in general by a thermal mixture [25], the calculation of an observable at time t can be done by a simple thermal average once $\Psi(x,z,t)$ is known (this averaging procedure is explained in section III, Eq. (19)). The two-dimensional Hamiltonian $\hat{\mathcal{H}}_{2\mathrm{D}}(x,z,t)$ can be written as the following sum

$$\hat{\mathcal{H}}_{2\mathrm{D}}(x,z,t) = \hat{T}_x + \hat{T}_z + V_g(x,z,t) + mgz\,, \tag{5}$$

where

$$\hat{T}_q = -\frac{\hbar^2}{2m}\frac{\partial^2}{\partial q^2} \tag{6}$$

denotes the kinetic energy operator along the q-coordinate.

The semi-classical approximation discussed above is introduced by replacing the z coordinate in the two-dimensional Hamiltonian $\hat{\mathcal{H}}_{2\mathrm{D}}(x,z,t)$ with the simple classical parameter $z_{ff}(t) = z_0 - \dot{z}_0 t - \frac{1}{2} g t^2$. The quantum dynamics of the atomic cloud along x is then described by the time-dependent Schrödinger equation for the wavepacket $\varphi(x,t)$

$$i\hbar \frac{\partial}{\partial t} \varphi(x,t) = \hat{\mathcal{H}}_{1\mathrm{D}}(x,t)\ \varphi(x,t)\,, \tag{7}$$

with a one-dimensional time-dependent Hamiltonian $\hat{\mathcal{H}}_{1\mathrm{D}}(x,t)$ given by

$$\hat{\mathcal{H}}_{1\mathrm{D}}(x,t) = \hat{T}_x + V_{1\mathrm{D}}(x,t)\,, \tag{8}$$

where $V_{1\mathrm{D}}(x,t) = V_g(x, z_{ff}(t), t)$. By adopting this one-dimensional approach, the numerical simulation is simplified at the cost of replacing the two-dimensional potential $V_g(x,z,t)$ (equations (1) and (2)) which is time-independent for $t > t_0$ with the time-varying one-dimensional potential $V_{1\mathrm{D}}(x,t)$. This potential changes slowly during the fall of the atom, and two of its snapshots are shown in the insets of Figure 1.

C. Time-dependent propagation

We assume the atom to be initially in a well defined vibrational level v_0 of the vertical guide potential $V_0(x)$

$$\varphi(x, t=0) = \chi_{v_0}(x)\,, \tag{9}$$

and we propagate the translational wavepacket in time until the date t_f corresponding to the altitude of the detection probe, using the splitting operator method developed by Feit *et al* [29]

$$\varphi(x, t+\delta t) = \mathrm{e}^{-i\hat{\mathcal{H}}_{1\mathrm{D}}\delta t/\hbar}\,\varphi(x,t)\,. \tag{10}$$

The total Hamiltonian $\hat{\mathcal{H}}_{1\mathrm{D}}(x,t)$ is splitted in two parts corresponding to the kinetic and potential propagators

$$\mathrm{e}^{-i\hat{\mathcal{H}}_{1\mathrm{D}}\delta t/\hbar} = \mathrm{e}^{-i\hat{T}_x\delta t/\hbar} \times \mathrm{e}^{-iV_{1\mathrm{D}}(x,t)\delta t/\hbar} \times \mathrm{e}^{-i\hat{T}_x\delta t/\hbar} \tag{11}$$

to decrease the error to the order $(\delta t)^3$. The kinetic propagation is performed in the momentum space, and the potential propagation in the coordinate space. Fast Fourier Transformation (FFT) allows rapid passage back and forth from one representation to the other at each time step. Typical grids extend from $x_{min} = -1.0\,\mathrm{mm}$ to $x_{max} = 2.0\,\mathrm{mm}$ with $N = 2^{20}$ grid points, and a time step of the order of $\delta t \simeq 40\,\mu\mathrm{s}$ is used.

At the end of the propagation the wavefunction $\varphi(x,t_f)$ is analyzed to determine the efficiency of the beam splitter and to extract detailed information on the state of the atom in each branch of the laser guide.

D. Initial trapping of the atomic cloud

We assume the initial atomic cloud to be in a thermal state at temperature T_0 described by the usual Maxwell-Boltzmann phase-space probability distribution $W(x,z,\dot{x},\dot{z})$ defined by the following four-dimensional product

$$W(x,z,\dot{x},\dot{z}) = W_Q(x) \times W_Q(z) \times W_P(\dot{x}) \times W_P(\dot{z})\,, \tag{12}$$

where $W_Q(q)$ and $W_P(\dot{q})$ $(q = x, z)$ are the position and momentum distributions

$$\left\{ \begin{array}{rcl} W_Q(q) & = & \dfrac{1}{\sqrt{2\pi}\,\sigma_0}\ \ \mathrm{e}^{-\,q^2/\,2\sigma_0^2} \\ W_P(\dot{q}) & = & \sqrt{\dfrac{m}{2\pi\,k_{\mathrm{B}}T_0}}\ \ \mathrm{e}^{-\,m\dot{q}^2/\,2k_{\mathrm{B}}T_0} \end{array} \right. . \tag{13}$$

In this expression σ_0 characterizes the size of the cloud and k_B is the Boltzmann constant. When the vertical guide is suddenly switched on at time $t = 0$, only a fraction of the cold atoms are trapped in the dipole potential created by the laser beam intensity profile.

The total trapping probability $P_{\rm trap}$ can be calculated from the position and momentum distributions, assuming that for a given position x the atom is trapped if its kinetic energy E_x along this direction is lower than the binding energy $-V_0(x)$ of the potential. The integral over x leads to the following rapidly convergent expansion

$$P_{\rm trap} = \sum_{n=0}^{\infty} \left(-\frac{U_0}{k_B T_0}\right)^n \frac{\beta_n}{(2n+1)\,n!}\,, \qquad (14)$$

where

$$\beta_n = \frac{2\,w_0}{\left[w_0^2 + (4n+2)\sigma_0^2\right]^{1/2}} \sqrt{\frac{U_0}{\pi\,k_B T_0}}\,. \qquad (15)$$

This expression is the one-dimensional analogue of the well-known two dimensional probability given for example in [10, 30, 31]. It should be noticed here that the trapping probability only depends on the two following dimensionless ratios σ_0/w_0 and $U_0/k_B T_0$. This is a signature of the fact that the trapping probability can be expressed in a phase-space diagram as the overlap between the atomic cloud distribution and the trapping condition [30, 31].

The variation of the trapping probability with the ratio $U_0/k_B T_0$ is depicted in Figure 3. For a given U_0, the trapping probability changes very slowly with the temperature of the atomic cloud. In a real experiment, trapping occurs along both x and y, and $P_{\rm trap}^2$ is therefore shown in Figure 3 to compare with the measurement performed in [31] for the ratio $U_0/k_B T_0 = 1.3$. Finally, as one might intuitively guess, the trapping probability increases significantly when the size of the atomic cloud σ_0 decreases compared to the laser waist w_0 characterizing the size of the trapping potential.

Using arguments based on energy conservation, the probability for an atom to be trapped in a well defined initial vibrational state v_0 of total energy ε_0 can also be calculated using

$$P(v_0) = \frac{1}{\rho(\varepsilon_0)} \int_{-l_0}^{+l_0} W_Q(x)\, W_E\left(\varepsilon_0 - V_0(x)\right) dx\,, \qquad (16)$$

once the density of states $\rho(\varepsilon_0)$ in the potential $V_0(x)$ is known. The positions $x = \pm\, l_0$, corresponding to $2\,l_0^2 = w_0^2 \ln(-U_0/\varepsilon_0)$, are the left and right turning points of the level v_0, and

$$W_E(E) = \frac{{\rm e}^{-\,E\,/\,k_B T_0}}{\sqrt{\pi\,E\,k_B T_0}} \qquad (17)$$

is simply the analogue of $W_P(\dot{q})$, writen in terms of kinetic energy $E = \varepsilon_0 - V_0(x)$. The state-dependent probability $P(v_0)$ only depends on the three following dimensionless parameters: σ_0/w_0, $U_0/k_B T_0$ and ε_0/U_0. It finally satisfies the relation

$$P_{\rm trap} = \sum_{v_0} P(v_0)\,. \qquad (18)$$

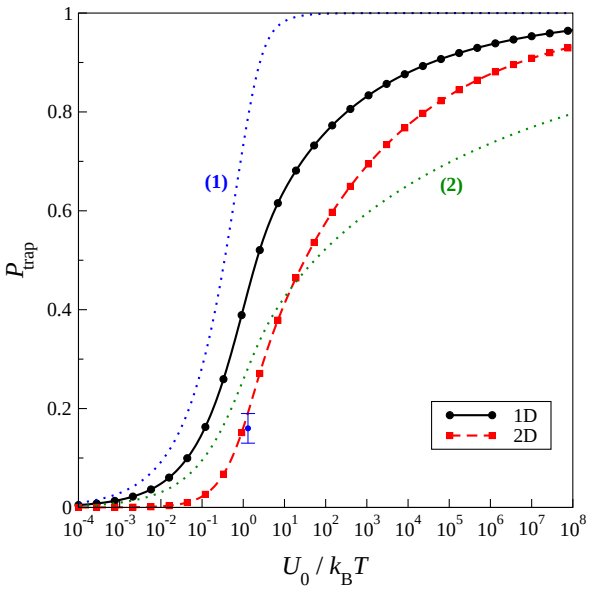

FIG. 3: (Color online) One-dimensional (black solid line) and two-dimensional (red dashed line) trapping probability as a function of the dimensionless ratio $U_0/k_B T_0$ (logarithmic scale) for $\sigma_0/w_0 = 1.5$. The blue point located at the abscise $U_0/k_B T_0 = 1.3$ with the error bar is an experimental measurement extracted from reference [31]. The one-dimensional trapping probabilities for $\sigma_0/w_0 = 0.5$ and 2.5 are also shown as blue and green dotted lines with the labels (1) and (2) respectively. All other parameters are as in Figure 2.

Figure 4 shows the initial distribution of vibrational levels for various ratios σ_0/w_0. The lowest levels dominate the distribution, and this is particularly true when the size of the atomic cloud σ_0 is smaller than the size of the trapping potential w_0. Just as with the total trapping probability $P_{\rm trap}$ shown in Figure 3, $P(v_0)$ changes very slowly with the temperature. This variation is therefore not shown here.

III. NUMERICAL RESULTS

A typical quantum dynamics can be seen Figure 5, which shows the time evolution of the initial level $v_0 = 6000$ as a function of x and z for the initial condition $z_0 = \dot{z}_0 = 0$. This initial state is a stationnary state of the vertical guide, and it does not evolve in time until it reaches the altitude $z_c = -4\,$mm where the two dipole guides cross. Afterwards, a wavepacket is created, and this one evolves inside two main branches, indicated by the white arrows. The oblique "trajectory" is guided

by the oblique laser beam represented by the thin white oblique dotted line, while in the vertical branch an oscillating wavepacket is evolving. The picture obtained here is not as simple as the classical trajectories shown in Figure 2 since this quantum state cannot be represented by a single trajectory. The consequence is that, depending on the initial conditions, the atomic wavepacket can be delocalized in the two guides simultaneously. A single initial quantum state can therefore split coherently along two paths separated by macroscopic distances. This effect, which is quantum by nature, might open some interesting perspectives for atom interferometry experiments with laser guides.

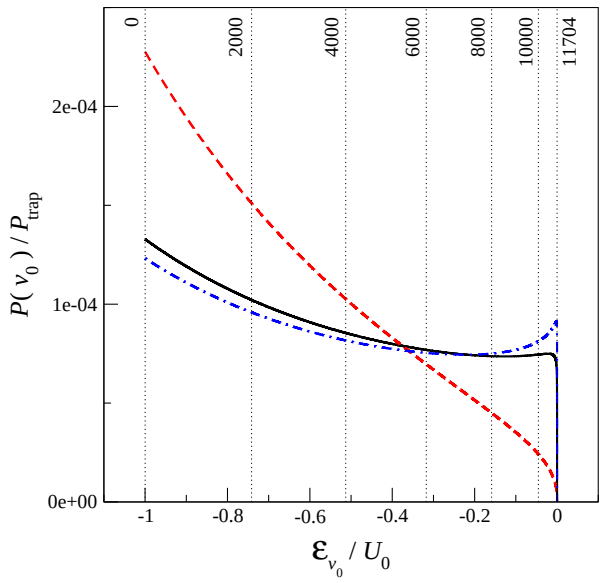

FIG. 4: (Color online) Initial population of the various vibrational levels $P(v_0)$ normalized with respect to the total trapping probability $P_{\rm trap}$ as a function of the ratio of their energy ε_0 to U_0. The black solid, red dashed and blue dash-dotted lines correspond to $\sigma_0/w_0 = 1.5$, 0.5 and 2.5 respectively. All other parameters are as in Figure 2. The energies of the levels $v_0 = 0$, 2000, 4000, 6000, 8000, 10000 and 11704 are indicated by the thin vertical dotted lines.

A realistic evaluation of the splitting efficiency between the two branches of the guide requires to take into account the position and momentum distributions of the atoms along x and z. The distribution along the direction x is described at the quantum level by solving the time-dependent Schrödinger equation (7) for a series of initial vibrational levels v_0. The distribution along z is taken into account classically by solving this equation for a series of initial classical conditions $(z_0, \dot{z}_0)$.

The splitting probability $P_s(v_0)$ of each initial trap state v_0 is then evaluated by calculating the probability of finding the atom in the right wing potential well, and thus in the oblique guide, at the altitude of the detection probe $z_p = -10\,\mathrm{mm}$

$$P_s(v_0) = P(v_0) \iint W_Q(z_0)\, W_P(\dot{z}_0) \times \int_{\substack{\text{Oblique}\\ \text{Guide}}} |\varphi_{z_0,\dot{z}_0}(x,t_f)|^2 \, dx \, dz_0 \, d\dot{z}_0 \,, \tag{19}$$

averaged over the initial distributions $W_Q(z_0)$ and $W_P(\dot{z}_0)$ [Eqs. (13)]. $P(v_0)$ denotes here the initial trapping probability of this state [Eq.(16)]. The wavepacket $\varphi_{z_0,\dot{z}_0}(x,t)$ is labelled here by the indexes $(z_0, \dot{z}_0)$ indicating the initial conditions of the simulation.

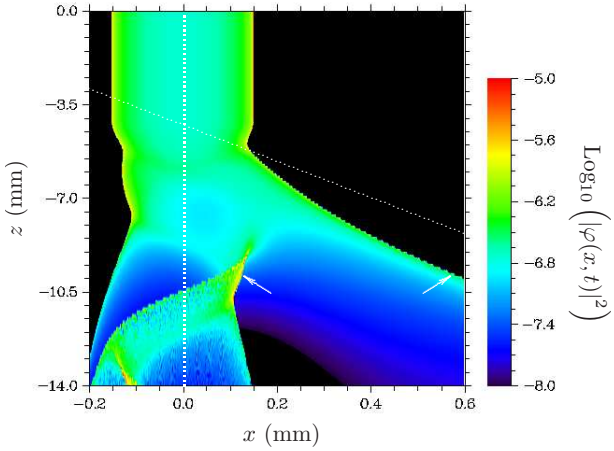

FIG. 5: (Color online) Contour plot depicting the time evolution of the envelope of $|\varphi(x,t)|^2$ on a logarithmic scale as a function of x and of $z(t) = z_0 - \dot{z}_0 t - \frac{1}{2}gt^2$. The atom is falling in the gravity field in the presence of the two trapping potentials with $U_0 = 30\,\mu$K, $U_1 = 10\,\mu$K, $w_0 = 0.2\,$mm and $w_1 = 0.3\,$mm. The two guides cross at the altitude $z_c = -4\,$mm with an angle $\gamma = 0.12\,$rad, and the oblique guide is switched on at $t_0 = 28.6\,$ms. The vertical and oblique dotted white lines reveal the directions of propagation of the laser beams. The two white arrows point to the location of the maximum probability density at the altitude $z = -10\,$mm. The initial level is here $v_0 = 6000$.

The "total" splitting efficiency P_s at temperature T_0 is finally evaluated by averaging over the vibrational quantum number v_0

$$P_s = \frac{1}{P_{\rm trap}} \sum_{v_0} P_s(v_0)\,, \tag{20}$$

where $P_{\rm trap}$ is the total trapping probability [Eq.(14)]. A unit splitting probability ($P_s = 1$) would indicate that all trapped atoms are captured by the oblique guide. A perfect beam splitter, whose reflection and transmission coefficients equal 0.5, corresponds to $P_s = 0.5$.

The state-dependent splitting probability $P_s(v_0)$ is shown Figure 6 as a function of v_0 for various sizes of the atomic cloud σ_0 at fixed temperature $T_0 = 14\,\mu$K.

Clearly, the lowest energy states ($v_0 \leqslant 3000$) are not deviated by the oblique guide, and they simply fall vertically. The explanation for this effect is simple: their

energy is too small to be trapped in the present oblique guide of depth $U_1 = 10\,\mu$K (see for instance the lower inset of Figure 1 representing the guiding potential around $z \simeq -8\,$mm). The eigenstates of vibrational quantum number higher than $v_0 \simeq 5800$ are the only states of total energy $\varepsilon_0 \geqslant -10\mu$K. In an energy-based first approximation, all states with $v_0 \leqslant 5800$ should therefore remain unaffected by the beam splitter. In reality, all vibrational states experience a quickly varying potential in the vicinity of z_c. They are therefore subjected to non-adiabatic transitions to higher or lower excited states which may or may not be captured in the oblique guide. Figure 6 shows that the states of vibrational quantum numbers $3000 \leqslant v_0 \leqslant 5800$ already have a significant probability of splitting. This non-adiabatic effect is especially important for the highest falling speeds, and thus for the initial conditions $z_0 > 0$ and $\dot{z}_0 \neq 0$.

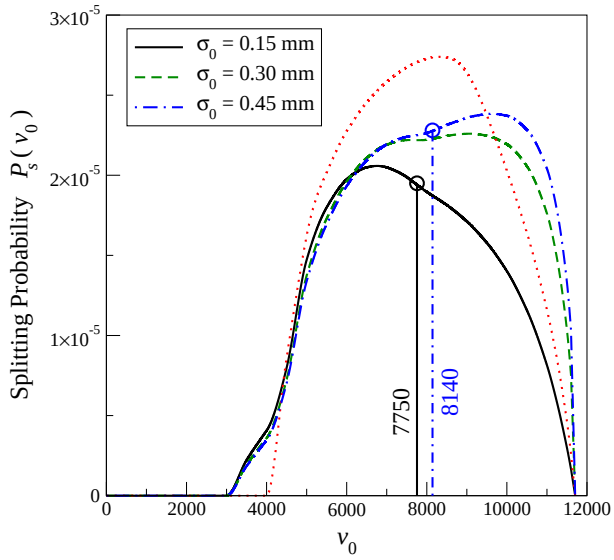

FIG. 6: (Color online) State-dependent splitting efficiency $P_s(v_0)$ as a function of the initial level v_0 for various sizes of the atomic cloud σ_0 and for $T_0 = 14\,\mu$K. The cloud sizes $\sigma_0 = 0.15$, 0.30 and 0.45 mm correspond to the solid black, dashed green and dash-dotted blue curves respectively. These probabilities have been averaged over the initial classical conditions chosen for z_0 and $\dot{z}_0$ (see Eq.(19)). The guide parameters are as in Figure 5. The two vertical lines indicate the average value of v_0 in the oblique guide for $\sigma_0 = 0.15\,$mm (black solid line), $\langle v_0 \rangle = 7750$, and $\sigma_0 = 0.45\,$mm (blue dash-dotted line), $\langle v_0 \rangle = 8140$. The red dotted curve shows the probability obtained with $\sigma_0 = 0.30$ mm for a single initial condition : $z_0 = \dot{z}_0 = 0$.

Another tendency can be noticed in this figure : larger atomic clouds, since they favor the initial trapping of higher vibrational levels in the vertical guide (see Figure 4 for instance), have a higher total splitting efficiency, and present a distribution of levels clearly shifted to higher energies. As a consequence, the average value $\langle v_0 \rangle$ of the trapped states is $\langle v_0 \rangle \simeq 7750$ for $\sigma_0 = 0.15\,$mm and $\langle v_0 \rangle \simeq 8140$ for $\sigma_0 = 0.45\,$mm.

A comparison of the probability distribution $P_s(v_0)$ obtained with $\sigma_0 = 0.30\,$mm when averaging over z_0 and $\dot{z}_0$ (dashed green curve in Figure 6) with the probability obtained for a single initial condition ($z_0 = \dot{z}_0 = 0$, red dotted curve in Figure 6) shows that even if the averaging procedure modifies significantly the probability distribution, a qualitatively correct description is already obtained by a single calculation where the atom is initially at rest, with $z_0 = \dot{z}_0 = 0$.

The total splitting efficiency P_s of the present beam splitter setup has been measured recently in Orsay for various altitudes of the crossing point z_c [31]. The conclusion of this experimental study is that, with the parameters chosen in Figure 7, a maximum splitting efficiency of about 10% should be observed around $z_c \simeq -6\,$mm. Some measurements made with a smaller waist w_1 and a higher potential depth U_1 also show that the variation of P_s with z_c is not symmetric with respect to its maximum value $z_c \simeq -6\,$mm. Our numerical study, which gives a maximum splitting probability of about 15% for the altitude $z_c \simeq -5.2\,$mm (see Figure 7) is therefore in qualitative agreement with this experimental measurement.

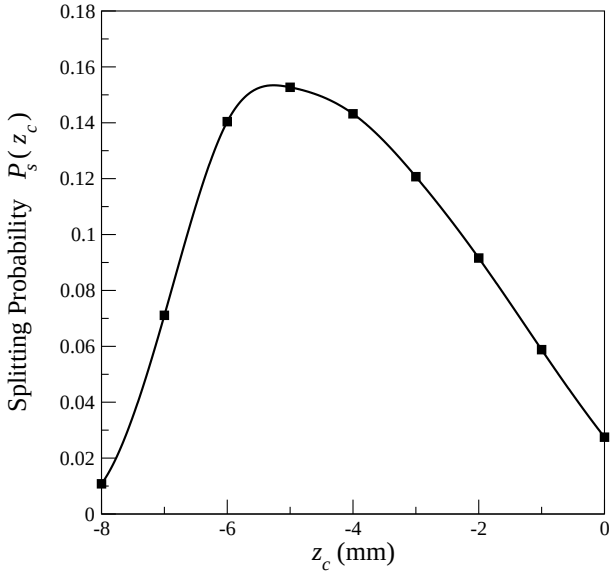

FIG. 7: Total splitting efficiency P_s [Eq.(20)] as a function of the crossing altitude z_c of the laser beams. This probability has been averaged over the initial conditions chosen for z_0 and $\dot{z}_0$, and summed over v_0. The size of the initial atomic cloud is $\sigma_0 = 0.30\,$mm. All other parameters are as in Figure 6.

The variation of the splitting probability with z_c can be explained as follows. If the average altitude of the atomic cloud is much smaller than the crossing altitude when the oblique guide is swiched on ($z_{ff}(t_0) \ll z_c$), the beam splitter is inefficient, as can be seen in Figure 7 for $z_c \gg -4\,$mm. On the opposite side of this graph, for $z_c \ll -4\,$mm, the oblique guide is on when the atoms reach z_c, but they reach this altitude with a kinetic energy which becomes comparable to – or higher than –

the binding energy of the oblique guide U_1. This explains why the efficiency of the beam splitter falls to 0 when $z_c \ll -4\,\mathrm{mm}$.

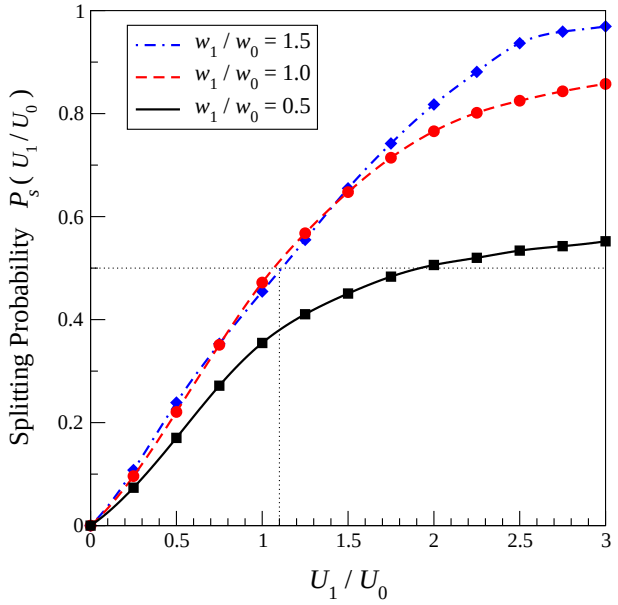

FIG. 8: (Color online) Total splitting efficiency P_s [Eq.(20)] for the initial conditions $z_0 = \dot{z}_0 = 0$ as a function of the ratio of the oblique to vertical potential depths U_1/U_0, and therefore as a function of the ratio of the beam intensities. For this calculation, U_0 is fixed (30 μK) and U_1 is varied. The crossing altitude between the two guides is $z_c = 4\,\mathrm{mm}$. The waist of the vertical beam is $w_0 = 0.2\,\mathrm{mm}$, and the splitting efficiencies calculated for an oblique waist of $w_1 = 0.1$, 0.2 and 0.3 mm are shown as black solid, red dashed and blue dash-dotted lines respectively. All other parameters are as in Figure 7.

Finally, we have calculated the variation of the total splitting efficiency P_s [Eq.(20)] of this beam splitter with one of the most crucial parameter : the potential depth of the oblique guide U_1. This numerical simulation has been performed for various ratios of oblique to vertical beam waists w_1/w_0. The result is shown in Figure 8 with fixed initial conditions $z_0 = \dot{z}_0 = 0$. One can notice here that the splitting efficiency varies monotonically from 0 to its maximum value when U_1 varies from 0 to $3\,U_0$. Depending on the value of the waist of the oblique guide, a total deflection of the beam can be realized (see for instance the case $w_1 = 1.5\,w_0$ and $U_1 = 3\,U_0$). A completely symmetric splitting is also predicted when $U_1 \simeq 1.1\,U_0$ and $w_1 \geqslant w_0$. This last prediction is in agreement with the experiment [31]. Finally, when the oblique guide is deep enough to induce a significant splitting of the atomic cloud, a higher splitting efficiency can be obtained by increasing w_1. The results shown in this figure indicate that a high degree of control exists in this type of experimental configuration since the splitting efficiency can be modified at will.

Figure 9 shows the average transverse energy (direc-

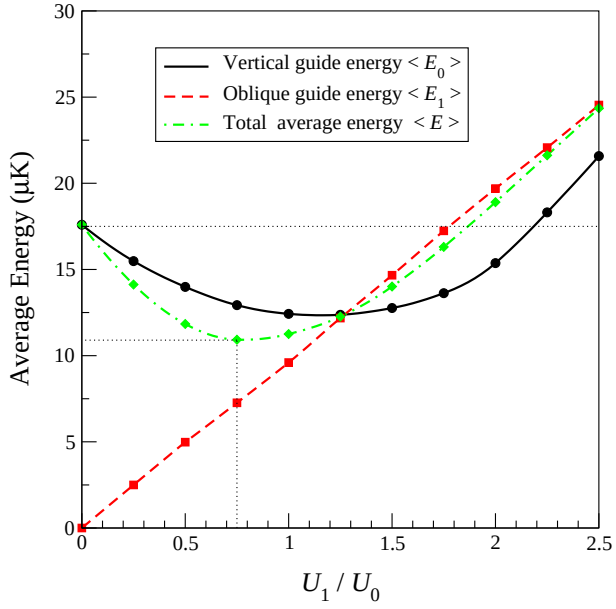

FIG. 9: (Color online) Average energies $\langle E_0\rangle$ (black solid line) and $\langle E_1\rangle$ (red dashed line) in the vertical and oblique guides as a function of U_1/U_0 for the initial conditions $z_0 = \dot{z}_0 = 0$. For this calculation, U_0 is fixed (30 μK) and U_1 is varied. The crossing altitude between the two guides is $z_c = 4\,\mathrm{mm}$. The waist of the vertical and oblique beams are $w_0 = 0.2\,\mathrm{mm}$ and $w_1 = 0.3\,\mathrm{mm}$. All other parameters are as in Figure 7. The total average energy $\langle E\rangle$ is also shown as a green dash-dotted line.

tions x and x') of the atoms in the vertical and in the oblique guide after the splitting : $\langle E_0\rangle$ and $\langle E_1\rangle$. An evaluation of the final energy $E_0(v_0)$ in the vertical guide is first performed for each initial state v_0 using the expression

$$E_0(v_0) = \int_{\substack{\text{Vertical}\\ \text{Guide}}} \varphi^*_{v_0}(x,t_f)\,\hat{\mathcal{H}}_{1\mathrm{D}}(x,t)\,\varphi_{v_0}(x,t_f)\,dx \quad (21)$$

This energy is then averaged over all vibrational levels

$$\langle E_0\rangle = \frac{\sum_{v_0} P(v_0)\,E_0(v_0)}{\sum_{v_0} P(v_0)\,P_0(v_0)}\,, \quad (22)$$

where

$$P_0(v_0) = \int_{\substack{\text{Vertical}\\ \text{Guide}}} \varphi^*_{v_0}(x,t_f)\;\varphi_{v_0}(x,t_f)\,dx \quad (23)$$

is the probability of experiencing a simple vertical fall when starting in the initial level v_0. In the oblique guide, a similar approach is used to calculate the average energy $\langle E_1\rangle$, but the transverse direction is now x'. A rotation of the reference frame is therefore in order. For this calculation, the wavefunction $\varphi_{v_0}(x,t_f)$ and the Hamiltonian $\hat{\mathcal{H}}_{1\mathrm{D}}(x,t)$ in Eq.(21) are thus replaced by

$$\begin{cases} \widetilde{\varphi}_{v_0}(x',t_f) \;\equiv\; \mathrm{e}^{i\,[m\,\dot{z}(t)\,\tan\gamma]\,x}\;\varphi_{v_0}(x',t_f) \\ \widetilde{\mathcal{H}}_{1\mathrm{D}}(x',t) \;\equiv\; \hat{\mathcal{H}}_{1\mathrm{D}}(x',t) + m\,g\,\sin\gamma\,x' \end{cases} \quad (24)$$

In parallel with the vertical and oblique average energies, Figure 9 also shows the total average energy $\langle E \rangle$ of the trapped atoms after the splitting. This quantity is calculated from $\langle E_0 \rangle$, $\langle E_1 \rangle$, and the total splitting probability P_s [Eq.(20)]

$$\langle E \rangle = (1 - P_s) \langle E_0 \rangle + P_s \langle E_1 \rangle \ . \tag{25}$$

For $U_1 = 0$, no deviation of the cloud is observed, and we obtain $P_s = 0$ and $\langle E \rangle = \langle E_0 \rangle$. This average transverse energy is in fact equal to the initial transverse energy of the trapped atoms ($17.5\,\mu$K). This behavior can be seen on the left part of Figure 9.

When U_1 increases by a small amount ($U_1 \leqslant U_0$) the highest vibrational levels of the vertical guide are deviated in the oblique potential (see Figure 6 for instance), and the average transverse energy of the atoms remaining in the vertical guide therefore decreases. A striking counter-intuitive effect is that the atoms which are deviated also have a translational energy which is smaller than the initial average energy of the trapped atoms. This happens because these high vibrational levels are now trapped in a weakly binding potential of depth $U_1 \leqslant U_0$. As a consequence, the total average translational energy $\langle E \rangle$ of the atoms in their transverse direction decreases after the splitting of the cloud. With the parameters used in Figure 9, a minimum energy of $10.9\,\mu$K is obtained for $U_1 \simeq 0.75\,U_0$, to be compared with the initial average energy of about $17.5\,\mu$K. A significant cooling effect is therefore obtained in the transverse direction, at the cost of a significant heating in the vertical direction.

Finally, on the right hand side of this figure, with very deep oblique potentials ($U_1 \geqslant 2\,U_0$), the atom temperature in the transverse direction exceeds the initial average energy of $17.5\,\mu$K. In this case, a heating process takes place due to the fact that the atoms are now trapped in a much deeper potential.

IV. CONCLUSION

We have proposed a theoretical model for the study of cold atom beam splitters. This model has a wide range of possible applications since it could be used, for instance, to describe the dynamics of cold atoms manipulated with atom chips. We have used this time-dependent semi-classical model to describe the atomic dynamics with two crossing dipole guides. We have taken into account the gravity, as well as the thermal population of the initial atomic cloud in order to compute the splitting efficiency of the beam splitter.

Our results are in good agreement with recent experimental measurements, and we have presented the influence of the main parameters on the atomic dynamics in this guiding and splitting configuration. We have shown that some eigenstates of the system split coherently in the two branches of the guide, and that different average temperatures can be obtained in the different arms of the beam splitter. An efficient cooling of the atoms is also predicted in the transverse direction.

All these results indicate that a high degree of control can be achieved in this type of cold atom beam splitters using simple gaussian laser beams. These techniques, applied to Bose-Einstein condensates and combined with the very impressive capabilities of spatial light modulators [32], should allow for the implementation of new exciting experimental schemes in the domain of atom optics and matter-wave interferometry.

Acknowledgments

We thank Hervé Le Rouzo for stimulating and helpful discussions. The IDRIS-CNRS supercomputer center supported this study by providing computational time under project number 08/051848. This work has been done with the financial support of the LRC of the CEA, under contract number DSM 05–33. Laboratoire de Photophysique Moléculaire and Laboratoire Aimé Cotton are associated to Université Paris-Sud.

[1] C. S. Adams, M. Sigel, and J. Mlynek, Phys. Rep. **240**, 143 (1994).
[2] S. Chu, Rev. Mod. Phys. **70**, 685 (1998).
[3] C. Cohen-Tannoudji, Rev. Mod. Phys. **70**, 707 (1998).
[4] W. D. Phillips, Rev. Mod. Phys. **70**, 721 (1998).
[5] C. E. Wieman, D. E. Pritchard and D. J. Wineland, Rev. Mod. Phys. **71**, S253 (1999).
[6] O. Houde, D. Kadio and L. Pruvost, Phys. Rev. Lett. **85**, 5543 (2000).
[7] S. Kuhr, W. Alt, D. Schrader, M. Müller, V. Gomer and D. Mechede, Science **293**, 278 (2001).
[8] T. L. Gustavson, A. P. Chikkatur, A. E. Leanhardt, A. Görlitz, S. Gupta, D. E. Pritchard and W. Ketterle, Phys. Rev. Lett. **88**, 020401 (2002).
[9] R. Dumke, T. Muether, M. Volk, W. Ertmer and G. Birkl, Phys. Rev. Lett. **89**, 220402 (2002).
[10] B. T. Wolschrijn, R. A. Cornelussen, R. J. C. Spreeuw and H. B. van Linden van den Heuvell, New J. Phys. **4**, 69.1 (2002).
[11] *Matter Wave Interferometry*, Ed. by G. Badurek, H. Rauch, and A. Zeilinger, North Holland Physics Publishing Division, Amsterdam (1988).

[12] *Atom Interferometry*, Ed. by P. Berman, Academic Press, New York (1997).
[13] D. Jaksch, H. J. Briegel, J. I. Cirac, C. W. Gardiner and P. Zoller, Phys. Rev. Lett. **82**, 1975 (1999).
[14] A. Hemmerich, Phys. Rev. A **60**, 943 (1999).
[15] G. Brennen, C. M. Caves, P. S. Jessen and I. H. Deutsch, Phys. Rev. Lett. **82**, 1060 (1999).
[16] T. Calarco, E. A. Hinds, D. Jaksch, J. Schmiedmayer, J. I. Cirac and P. Zoller, Phys. Rev. A **61**, 022304 (2000).
[17] E. Charron, E. Tiesinga, F. Mies, and C. J. Williams, Phys. Rev. Lett. **88**, 077901 (2002).
[18] O. Mandel, M. Greiner, A. Widera, T. Rom, T. W. Hänsch and I. Bloch, Nature **425**, 937 (2003).
[19] J. V. Porto, S. Rolston, B. Laburthe Tolra, C. J. Williams and W. D. Phillips, Phil. Trans. R. Soc. Lond. A **361**, 1417 (2003).
[20] Y. Shin, M. Saba, T. A. Pasquini,W. Ketterle, D. E. Pritchard, and A. E. Leanhardtr, Phys. Rev. Lett. **92**, 050405 (2004).
[21] D. Müller, E. Cornell, M. Prevedelli, P. Schwindt, A. Zozulya, and D. Anderson, Opt. Lett. **25**, 1382 (2000).
[22] D. Cassettari, B. Hessmo, R. Folman, T. Maier, and J. Schmiedmayer, Phys. Rev. Lett. **85**, 5483 (2000).
[23] D. Müller, E. A. Cornell, M. Prevedelli, P. D. D. Schwindt, Y.-J. Wang, and D. Z. Anderson, Phys. Rev. A **63**, 041602 (2001).
[24] P. Hommelhoff, W. Hänsel, T. Steinmetz, T. W. Hänsch, and J. Reichel, New J. Phys. **7**, 3 (2005).
[25] H. Kreutzmann, U.V. Poulsen, M. Lewenstein, R. Dumke, W. Ertmer, G. Birkl and A. Sanpera Phys. Rev. Lett. **92**, 163201 (2004).
[26] J. A. Stickney and A. A. Zozulya, Phys. Rev. A **68**, 013611 (2003).
[27] D. C. E. Bortolotti and J. L. Bohn, Phys. Rev. A **69**, 033607 (2004).
[28] R. W. Brankin and I. Gladwell, Annals of Numer. Math. **1**, 363 (1994).
[29] M. J. Feit, J. A. Fleck and A. Steiger, J. Comput. Phys. **47**, 412 (1982).
[30] L. Pruvost, D. Marescaux, O. Houde and H. T. Duong Opt. Comm. **166**, 199, (1999).
[31] O. Houde, PhD Thesis, http://www.lac.u-psud.fr/theses-lac/Olivier%20Houde/DocFinal.pdf, Chapter 1, Université Paris Sud, December 2002.
[32] D. McGloin, G. C. Spalding, H. Melville, W. Sibbett and K. Dholakia, Opt. Express **11**, 158 (2003).